International Journal of Bifurcation and Chaos, Vol. 19, No. 3 (2009) 993–1006


# ANALYSIS AND MODELING OF AN EXPERIMENTAL DEVICE BY FINITE-TIME LYAPUNOV EXPONENT METHOD

N. SANTITISSADEEKORN*, D. BOHL† and E. M. BOLLT*
*Department of Mathematics and Computer Science, Clarkson University, Potsdam, NY 13699-5815, USA
†Department of Mechanical and Aeronautical Engineering, Clarkson University, Potsdam, NY 13699-5815, USA

Received October 30, 2007; Revised December 4, 2007

In this paper, we investigate the transport and mixing process of the batch mixers with two different configurations, the centered-blade and offset-blade mixers, by using a dynamical system approach. The 2-D velocity fields of the mixers measured using Particle Image Velocimetry (PIV) are used to identify the Lagrangian coherent structures (LCSs). The results show that the LCSs separate the physical space into two portions. In the case of the center-blade mixer the portion bounded inside the LCS experiences a relatively slow mixing relative to the portion outside of the LCS boundary. However, when the blade position is located near the wall, the LCS becomes more complicated but it still separates regions of fast mixing from a slower one. We develop a heuristic dynamical system model of our mixers to understand how the vorticity strength at the blade tips influences the variation of the LCSs. Finally, we define an appropriate notion of mixing to study the mixing rate of our mixing devices.

*Keywords*: Finite-time Lyapunov exponent; Lagrangian coherent structures; transport and mixing; fluid mixing.

## 1. Introduction

The Navy has an expressed interest in increasing the safety of its shipboard energetic materials (i.e. explosives, propellants, pyrotechnics). This desire has been driven by past accidents involving energetic materials, such as the USS Forrestal fire in 1967. The safety of such materials depends upon both the components in the formulation as well as in the uniformity of the mixing during production. In the mixing process of solid particles, which can be energetic crystals, solid oxydizers, or solid fuels, there is a need for uniform distribution within a highly viscous polymer. Like many other polymer based materials, energetic materials are often manufactured using batch (e.g. planetary) mixers. Batch mixers, which are similar to food mixers, are the primary method for the processing of energetic materials in the United States because they offer several advantages including: the possibility for long residence times (which increase the potential for uniform mixing), low damage potential to the energetic crystals, and the ability to add multiple ingredients relatively simply during processing. These advantages are balanced by the inherent drawbacks to a batch mixing process: inconsistent mixture quality, residual voids and fissures, lower allowed material viscosity which limits the solids that can be loaded into the mixture, limited pot life of the material being mixed, and the need for the use of environmentally hazardous solvents. While the use of batch mixers in industrial applications has a long history, the understanding of the physics

of mixing in these devices is limited. The flows are highly viscous, non-Newtonian, and particle laden which make them difficult to study. The experimental study of these devices is further complicated by complex geometries, and device scaling issues. Recent interest in developing more efficient, controllable mixing processes has focused attention on developing a better understanding on the physics of these devices. To facilitate improvements in designs and processes both experimental and computational approaches have been utilized. The development of computational tools is attractive in that such tools allow for relatively rapid and simple changes to both geometry and operating conditions to determine optimal mixing protocols. However, the development of computational tools has been hampered because of a lack of experimental data for model development and comparative validation.

Experimental work on batch mixers is somewhat limited [Zhou *et al.*, 2000; Tanguy *et al.*, 1996; Youcefi *et al.*, 1997; Bohl, 2007]. Recently researchers have begun to apply nonintrusive optical techniques to better understand the flow fields of industrial mixing devices [Bohl, 2007; Jaffer *et al.*, 2000; Bakalis & Karwe, 2002; Yoon *et al.*, 2005], however, there continues to be a lack of fundamental understanding of the fluid motions and mixing processes. The current work was undertaken in support of the development of computational tools for the modeling of low Reynolds number mixing devices. The goals of the experimental work were to: (1) map out local flow properties (e.g. the velocity, vorticity) to identify the fluid structures and inferred mixing potential in a simplified batch mixer, (2) determine the effects of Reynolds number on the flow structure, and (3) support the development of computational tools for the processing of energetic materials being carried out in parallel with this study. In the first phase, the code development motion of Newtonian fluids in a 2D flow field is to be calculated. This phase of the code work motivated the current work which investigates the flow field of a simple 2D mixer in a Newtonian fluid at low Reynolds number.

## 2. Experimental Methods

Details of the experimental methods can be found in [Bohl, 2007]. Figure 1 shows a schematic of the experimental apparatus. A clear acrylic cylindrical flat bottomed container was constructed with an inside radius of $r_w = 6.93\,\text{cm}$. A flat stainless steel blade was placed in the cylinder such that the long axis of the blade was parallel to the $z$-axis of the container. The blade had a width of $r_b = 2.99\,\text{cm}$ $(0.43\,r_w)$, a thickness of $0.14\,\text{cm}$ $(0.02\,r_w)$ and could be placed at various locations (i.e. offsets) with respect to the wall. The blade was rotated about its long axis by a DC motor to drive the fluid motion. The data presented in this paper used glycerin as the working fluid. The Reynolds number was $\text{Re} = 9$, with the Reynolds number defined as $\text{Re} = 2fr_w^2/\nu$ where $f$ is the rotational frequency

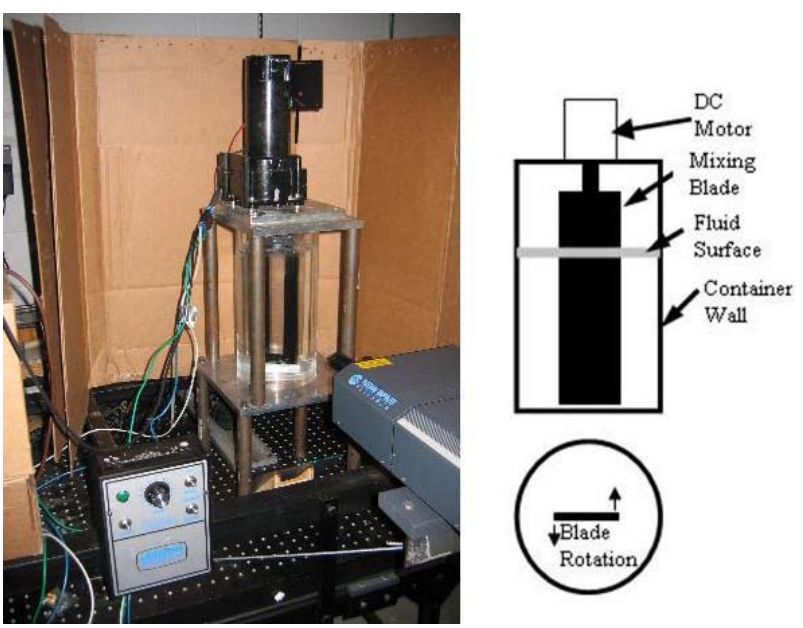


Fig. 1. Experimental mixing apparatus.

of the mixing blade. The geometry was chosen as a simplified first order model of a batch mixer to provide simple, well-defined boundary conditions that could be used to aid model development and provide validation data for the developed computational tools.

The 2D velocity fields were measured using Particle Image Velocimetry (PIV). Briefly, PIV relies on seed particles in a fluid that scatter light from a thin laser sheet created in the plane of interest. These particles may exist within the fluid naturally or be added to the fluid before measurements are made. The particles in the flow are imaged twice with a short, known delay between images. The displacement of the particles, or groups of particles, is determined via pattern matching techniques and a local velocity vector is calculated by dividing the displacement by time between images. The velocity can be determined at discrete points over the entire image and the 2D velocity field in the plane of the laser sheet can be assembled. Other kinematic quantities, such as vorticity, strain and stress, can then be calculated using the planar velocity field. A detailed discussion of PIV can be found in [Adrian, 2005].

In the current work, the working fluid was seeded with 10 micron silver coated glass spheres. Light was provided by a 4 Watt Spectra Physics Argon Ion laser. The mixing blades were painted with flat black paint to reduce the reflection of the laser sheet in the measurement region. The laser light was pulsed using a NM Laser Products fast mechanical shutter. This shutter had a minimum closed-open-closed cycle time of 1 msec. This was short enough that the imaged particles did not experience blurring during the exposure time. Images were capture using a Cooke Corporation Sensicam-QE CCD camera (8 bit, $1376 \times 1040$ pixels). The flow was viewed through the clear bottom of the container to provide data in a plane perpendicular to the long axis of the mixing blade (i.e. the $r$–$\theta$ plane).

The displacement of groups of particles was determined using the direct correlation technique described in [Gendrich & Koochesfahani, 1996]. Each FOV was approximately 8.7 cm $\times$ 12 cm in size (0.0087 cm/pixel). Delay times between the images were chosen to give maximum displacements of nominally 10 pixels and the source windows used in the correlation technique were $45 \times 45$ pixels with a 50% overlap. The error in the velocity measurements is limited by the ability to measure the displacement of the particles between images. The correlation technique used to process the data in this work is well documented and has a 95% uncertainly level of 0.1 pixel which corresponds to an uncertainty in the instantaneous velocity measurements of 0.08 cm/sec.

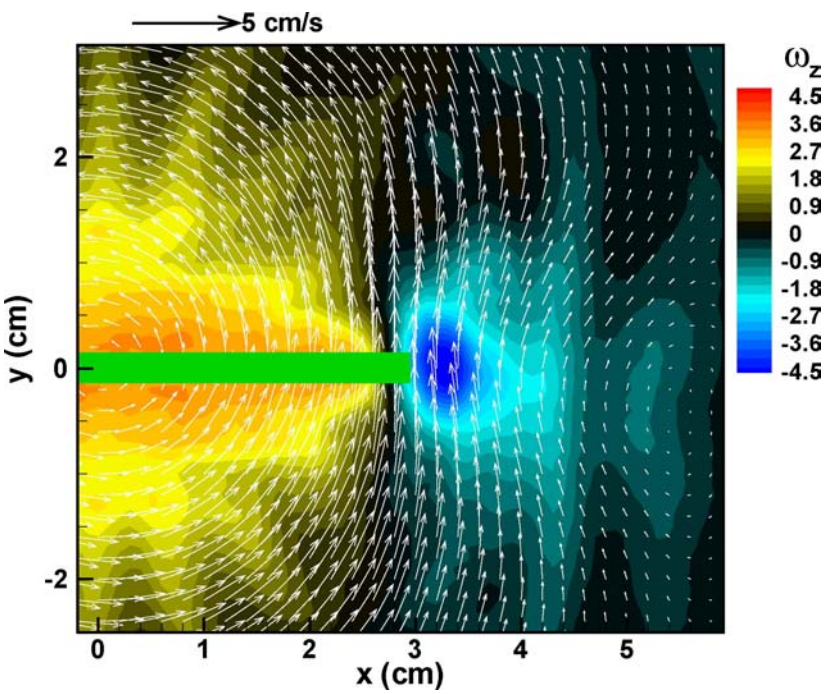


Fig. 2. Representative phase averaged velocity and vorticity fields from PIV data. Case shown is from the centered data.

The flow field under investigation was periodic in nature, with the periodicity linked to the motion of the mixing blade, which allowed the data to be phase averaged with respect to the motion of the blade. The blade phase, was defined such that 1/2 rotation was given for $\phi = 0$ to 1 (i.e. $\phi$ ranged from 0 to 2 for a complete blade rotation). This allowed data from multiple experiments and multiple Fields of View (FOV) to be combined to form a single data set. Phase averaging and the combining of multiple data sets allowed multiple individual measurements to be averaged for a single measurement location which reduces the estimated error in the presented data by a factor of 2 to 0.04 cm/sec. Local vorticity was calculated using a second order finite difference method using the spatially nearest velocity measurements. Vorticity error values were estimated to be 0.38 and 0.16 $\text{sec}^{-1}$ for the high and low frequency cases respectively. All data presented in this work are from PIV measurements taken at the mid-height of the fluid column. Data not shown here indicate that the flow field was independent of the $z$-location over the middle half of the mixing blade.

Representative phase averaged velocity and corresponding vorticity fields from the PIV data are shown in Fig. 2 for the centered blade case. Of note in this figure is the strong vortex that forms near the tip of the blade and travels with the blade as it sweeps through the fluid. A second region of vorticity forms along the blade surface and along the container bounding wall. A region of reverse flow is observed between the tip vortex and the bounding wall. Detailed discussion of this flow field can be found in [Bohl, 2007].

## 3. Transport and Mixing in the Mixers

In this section we demonstrate an analysis of transport and mixing for our rotating flat plate mixer by approximating the Lagrangian coherent structure (LCS) based on the finite-time Lyapunov exponent (FTLE) [Haller & Poje, 1998; Haller, 2000, 2002]. For a steady flow, the LCSs, extracted from the FTLE field, approximate stable and unstable invariant manifolds of a hyperbolic fix point, which separate regions exhibiting qualitatively different activities. In general, LCSs have one less dimension than the dimension of a domain of a dynamical system and they constitute pseudo-barriers to transport and mixing; the flux of particles across an LCS approaches zero as the integration time for computation of the FTLE becomes larger [Shadden *et al.*, 2005, 2006]. We intend to use these analytical tools to quantify mixing in various notions to study mechanisms enhancement and/or inhibition of mixing in future work. One of practical approaches to locate LCSs is to compute the FTLE of a time-dependent velocity field, the local stretch rate over a finite-time interval [Haller, 2000, 2002]. We consider a two-dimensional velocity field on $M \subset \Re^2$

$$\begin{aligned} \frac{dx}{dt} &= u(x, y, t) \\ \frac{dy}{dt} &= v(x, y, t), \end{aligned} \tag{1}$$

where $\mathbf{v} \equiv (u(x, y, t), v(x, y, t))$ is at least $C^2(M)$. Hence we can integrate this velocity field to obtain the flow map $\phi_\tau : \mathbf{x}(t) \mapsto \mathbf{x}(t + \tau)$. The finite-time strain tensor of the velocity field along the trajectory $\mathbf{x}(t)$ is given by the the symmetric, time-dependent, $2 \times 2$ matrix

$$J_\tau = \frac{d\phi_\tau \mathbf{x}(t)}{d\mathbf{x}}^* \frac{d\phi_\tau \mathbf{x}(t)}{d\mathbf{x}}, \tag{2}$$

where $A^*$ denotes the adjoint of $A$. We assume that on some finite time interval, the minimum and maximum eigenvalues, $\lambda_{\min}(\tau)$ and $\lambda_{\max}(\tau)$, of $J_\tau$ satisfy the condition:

$$\ln \lambda_{\min}(\tau) < 0 < \ln \lambda_{\max}(\tau). \tag{3}$$

This condition implies that there are both compression in one direction and expansion in the other along the trajectory. This type of trajectory of a time dependent velocity field is refereed to as a *hyperbolic trajectory* [Wiggins, 2003]. Also, we recall that the spectral norm of the Jacobian $d\phi_\tau \mathbf{x}(t)/d\mathbf{x}$ is given by

$$\left\| \frac{d\phi_\tau \mathbf{x}(t)}{d\mathbf{x}} \right\|^2 = \lambda_{\max}(\tau) \tag{4}$$

The FTLE, which represents the maximum stretching at the point $\mathbf{x}(t)$ along the trajectory with duration time $\tau$, is given by

$$\sigma_\tau(\mathbf{x}(t)) = \frac{1}{|\tau|} \ln \sqrt{\lambda_{\max}(\tau)}. \tag{5}$$

One can define repelling and attracting LCSs according to [Haller, 2002; Shadden *et al.*, 2005] as the maximum ridges of FTLE computed in forward time ($\tau > 0$) and backward time ($\tau < 0$), respectively.

The PIV output provides discrete measurements of the velocity field over a plane at finite times which can be used to compute the FTLE based on Eq. (5). However, an interpolation is needed to integrate points where the velocity field is not given in the PIV data. Furthermore, if the time step for the integration is smaller than the duration of two consecutive experimental time steps, we have to assume that the variation of velocity fields between two consecutive velocity data is small so that an interpolation in the time domain is also suitable. Conditions for the existence of finite-time hyperbolic trajectory can be found in [Haller & Poje, 1998].

Figure 3 shows snapshots of the forward-time FTLE of the mixer with the blade positioned at the center. We set the integrating time to half of a full rotation, $\tau = 2.1342$ seconds. Note that one period of the vector field here is half of a full revolution of the blade since there is no distinction between the two tips of the blade. Numerically, at each time $t$, we integrate samples of grid points by a fourth-order Runge–Kutta method to find their positions at time $t+\tau$. The cubic method is used for an interpolation during the integration. Then, we compute the spatial gradient of the flow $d\phi_\tau \mathbf{x}(t)/d\mathbf{x}$ by a central-difference scheme at each initial grid points. The FTLE at time $t$ for each initial point can be

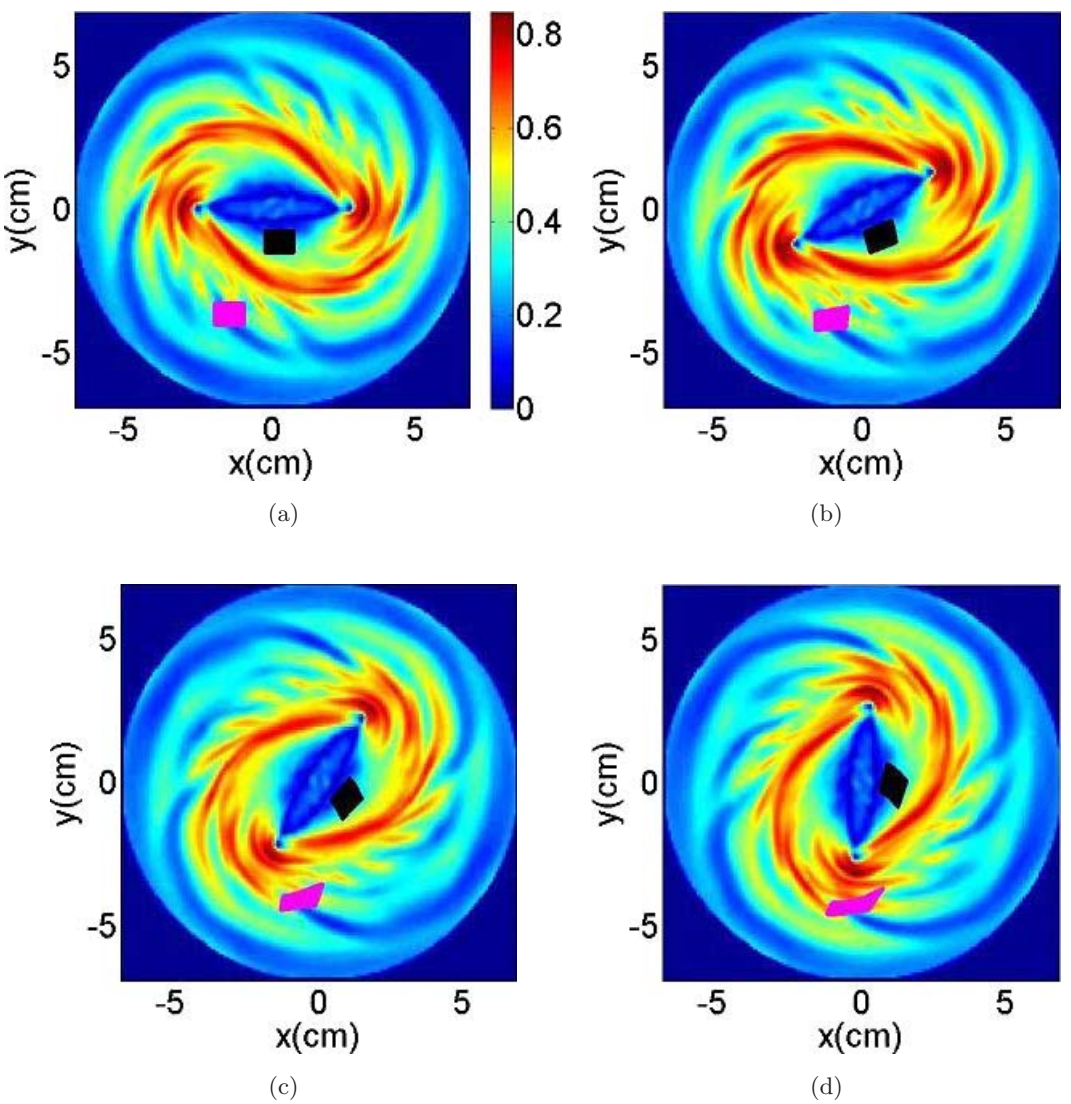


Fig. 3. The forward-time FTLE field of the mixer with the centered blade is computed at different time $t$ with the integrating time $\tau = 64\triangle t$, where $\triangle t = 0.033$ seconds. From (a) to (f), the FTLE is computed at time $t = \triangle t$, $t = 10\triangle t$, $t = 20\triangle t$, $t = 30\triangle t$, $t = 40\triangle t$ and $t = 60\triangle t$, respectively. The initial particles are placed to straddle the LCS and they are advected to demonstrate that the resulting LCSs serve as the transport barrier.

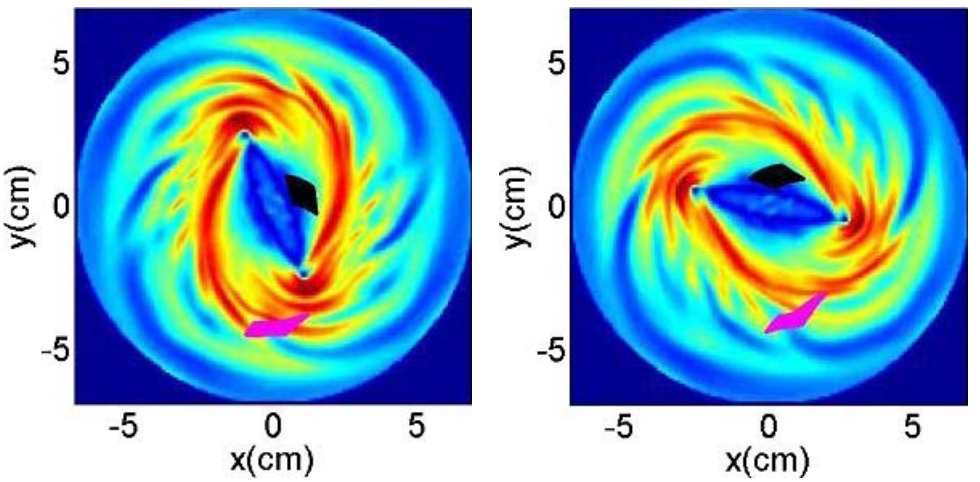


(e) (f)

Fig. 3. (*Continued*)

evaluated according to Eq. (5). The SVD is used to compute the eigenvalues of Eq. (2).

The LCS of the flow can be defined as ridges of the FTLE field as shown in Figs. 3 and 4. We observe the Lagrangian property of the LCS by tracing the trajectory of particles straddling the LCS. One can see that these particles do not transverse the LCS. In order to understand the motion differences between the two regions separated by the LCS, we use the particle tracers shown in Fig. 5 to visualize the geometry of the flow. This further suggests that the repelling LCS divide the space mainly into two regions; the region surrounded by the repelling LCSs experiences a very low degree of mixing whereas a higher degree of mixing occurs in the "outside" region. Furthermore, we compute the backward-time FTLE of the flow of the same mixer. Recall that the backward-time FTLE reveals to us the attracting LCSs, which is a finite-time version of an unstable manifold of a steady flow. Therefore, the particles tend to accumulate along the attracting LCSs as observed in Fig. 4. With the aid of these forward and backward time FTLE, we see that the stable and unstable of periodic points form a trapping region (Fig. 6) that traps fluid particles inside itself and hence mixing has a potential to occur only between the particles in the trapping region. Notice that the boundary of the trapping region moves along with the rotation of the blade tips and also that the center point of the mixer is a hyperbolic fixed point that is responsible for mixing inside the trapping region.

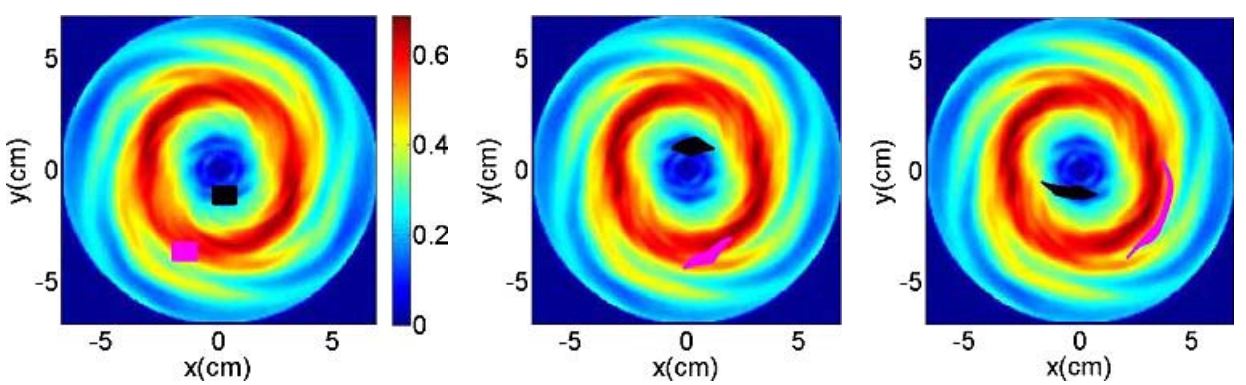


(a) (b) (c)

Fig. 4. The backward-time FTLE field of the mixer with the centered blade is computed at different time $t$ with the integrating time $\tau = 64\triangle t$ as in Fig. 3. From (a) to (c), the FTLE is computed at time $t = \triangle t$, $t = 60\triangle t$ and $t = \tau + 60\triangle t$, respectively. Here we observe that the initial particles are colored by the magenta accumulated along the ridge of the FTLE field. Thus the ridge of the backward-time FTLE field may be regarded as an unstable manifold.

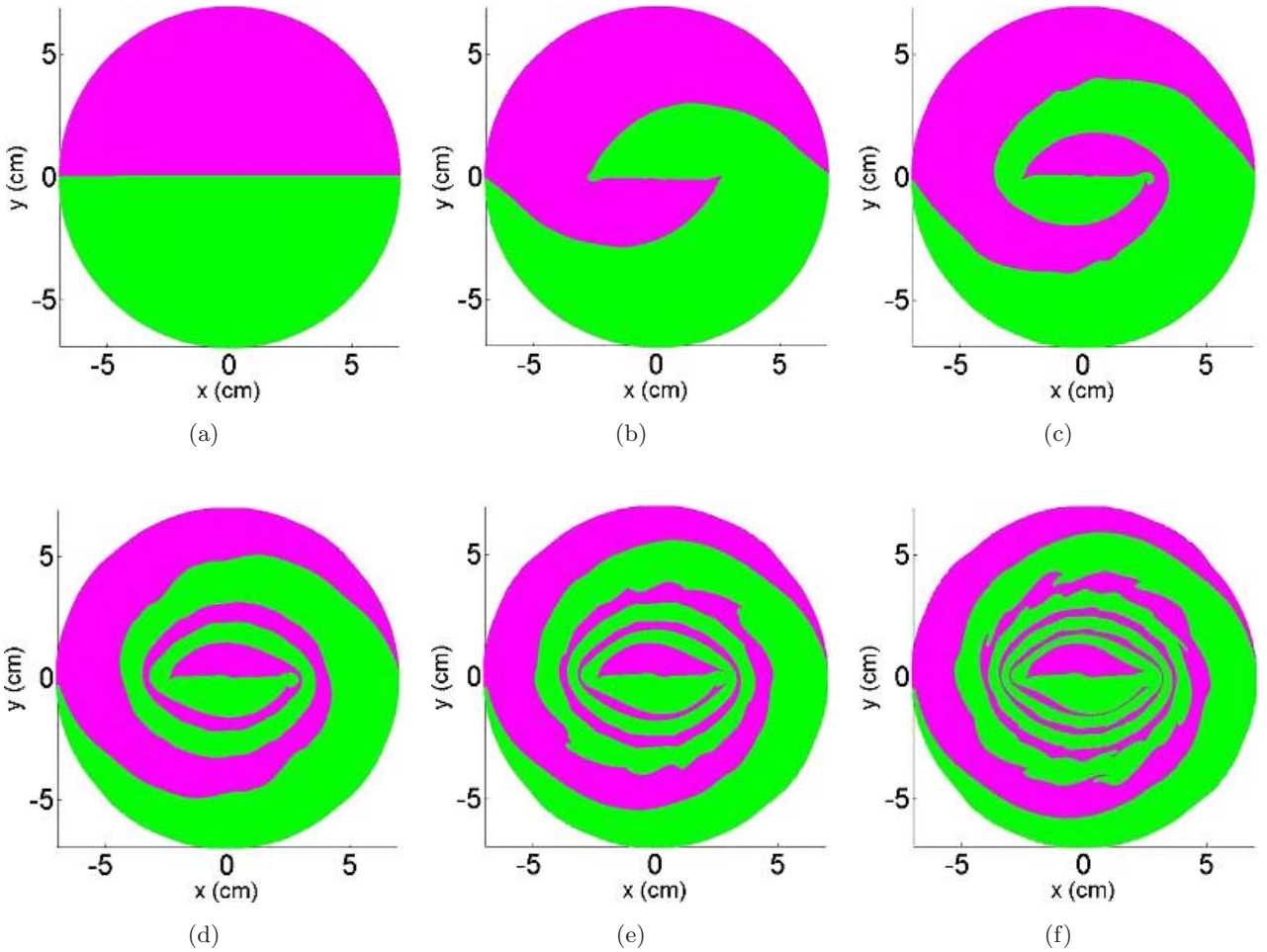


Fig. 5. Snapshots of particle tracers for the mixer with the centered blade. Two sets are particles, A (green) and B (magenta) are initially separated to occupy half of the physical space as shown (a). The initial particle distribution is then allowed to change as dictated by the flow field for 1, 2, 3, 4, and 5 periods, (b)–(f), respectively.

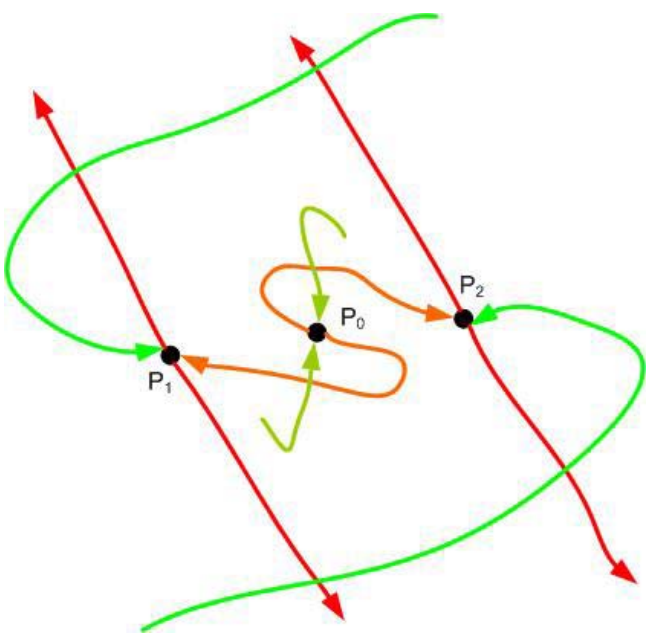


Fig. 6. A heuristic rendering to a stable and unstable heteroclinic tangle made of the mixing system inferred from the observed time-dependent LCS structures. The periodic points $P_1$ and $P_2$ correspond to the blade tips. The forward and backward time FTLE fields in Figs. 3 and 4 suggest that the transverse intersection by the stable and unstable manifolds of $P_1$ and $P_2$ generate a trapping region that bounds the trajectories of particles within this cell. Note that the mixing inside the trapping region is a result of the hyperbolic fixed point at the center of the mixer.

We point out that the velocity field of our mixer may be considered as a periodically perturbed Hamiltonian system. For such a system, it is well-known that the stable and unstable manifolds have an infinite length in general [Wiggins, 2003]. Therefore, we should expect the resulting LCS to be revealed more as the integrating time increases. However, this requires higher resolutions of sample points and hence a longer computational time, see Fig. 7. One can see stretching and folding of "stripes" in the mixer, which suggests a need of a larger number of grid points to compute the FTLE as the integrating time is increased.

We observe that FTLE fields for the mixer with the offset blade, Fig. 8, reflects a high degree of stretch near the wall where the tips of the blade rotate. Again, the LCS occurs on the boundary that separates strong and weak mixing as observed from the tracer plot in the figure. However, the mixed region in this case is smaller than that of the centered-blade mixer and it is the mixed region that is almost enclosed by the LCS instead of the region with a weak mixing as in the case of the centered blade. Also, we notice a vanishing of the LCS as one of the blade tips rotates away from the wall and it reappears when the other tip rotates toward the wall. Again, we observe the numerical displacement of the tracers to further understand the transport. It is shown in Fig. 9 that the LCSs in Fig. 8 separate the region of a relatively higher degree mixing within the sweep of the blade from that of a lower degree of mixing. This is different from the case of the centered-blade mixer in which the region bounded inside by the LCSs experience a lower degree of mixing than the other region. Furthermore, the particle striation in this case occurs in a more intricate fashion with a faster mixing rate than in the case of the centered-blade mixer. However, in this case the amount of particles that are mixed together is clearly less than that of

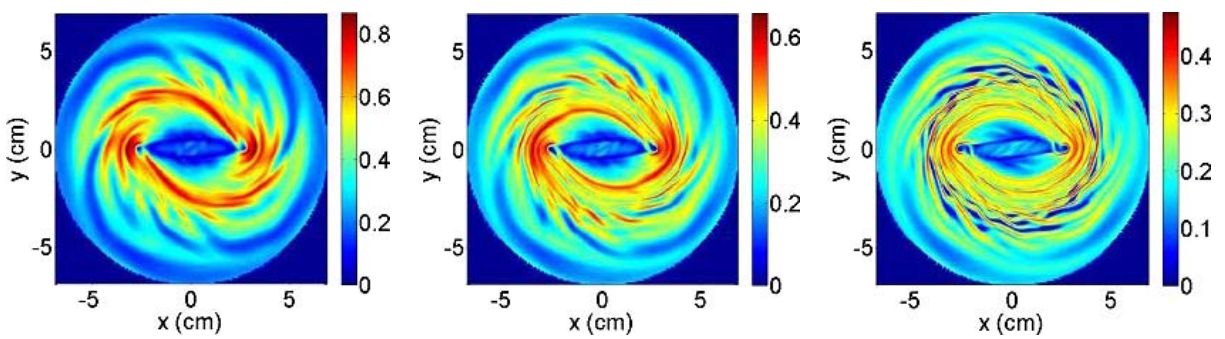


(a) (b) (c)

Fig. 7. Compute the FTLE fields with different integrating times, $\tau = T$, $\tau = 2T$ and $\tau = 4T$, respectively, where $T$ is the time for one period.

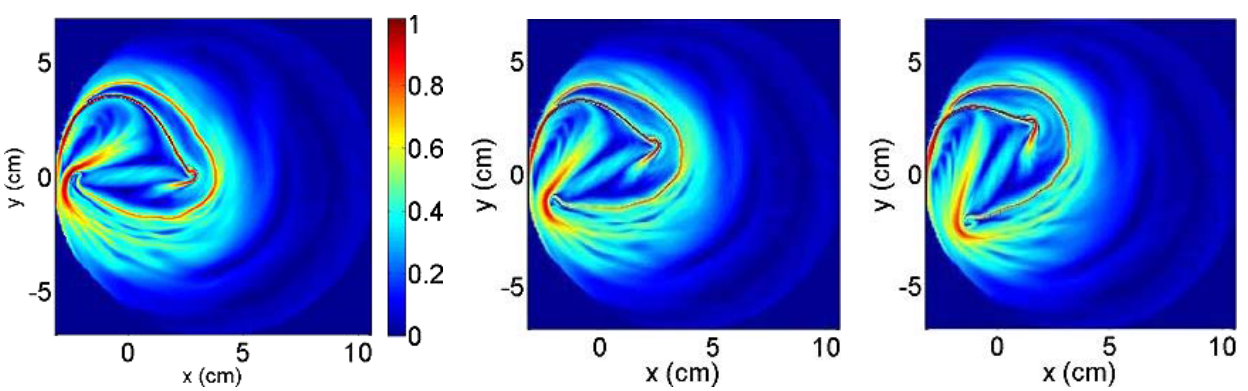


(a) (b) (c)

Fig. 8. The forward-time FTLE field of the mixer with the offset blade is computed at different times $t$ with the integrating time $\tau = 64\triangle t$. From (a) to (f), the FTLE is computed at time $t = \triangle t$, $t = 10\triangle t$, $t = 20\triangle t$, $t = 30\triangle t$, $t = 40\triangle t$ and $t = 50\triangle t$, respectively.

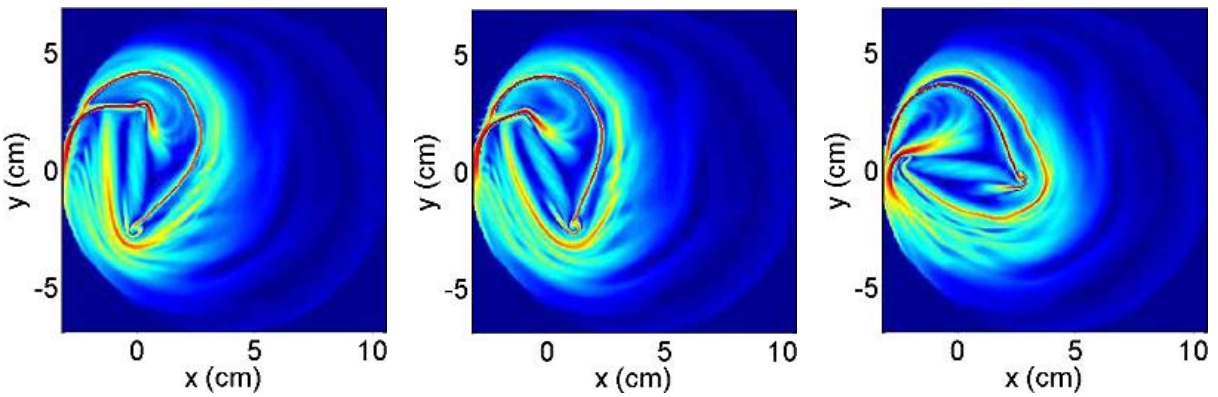


(d) (e) (f)

Fig. 8. (*Continued*)

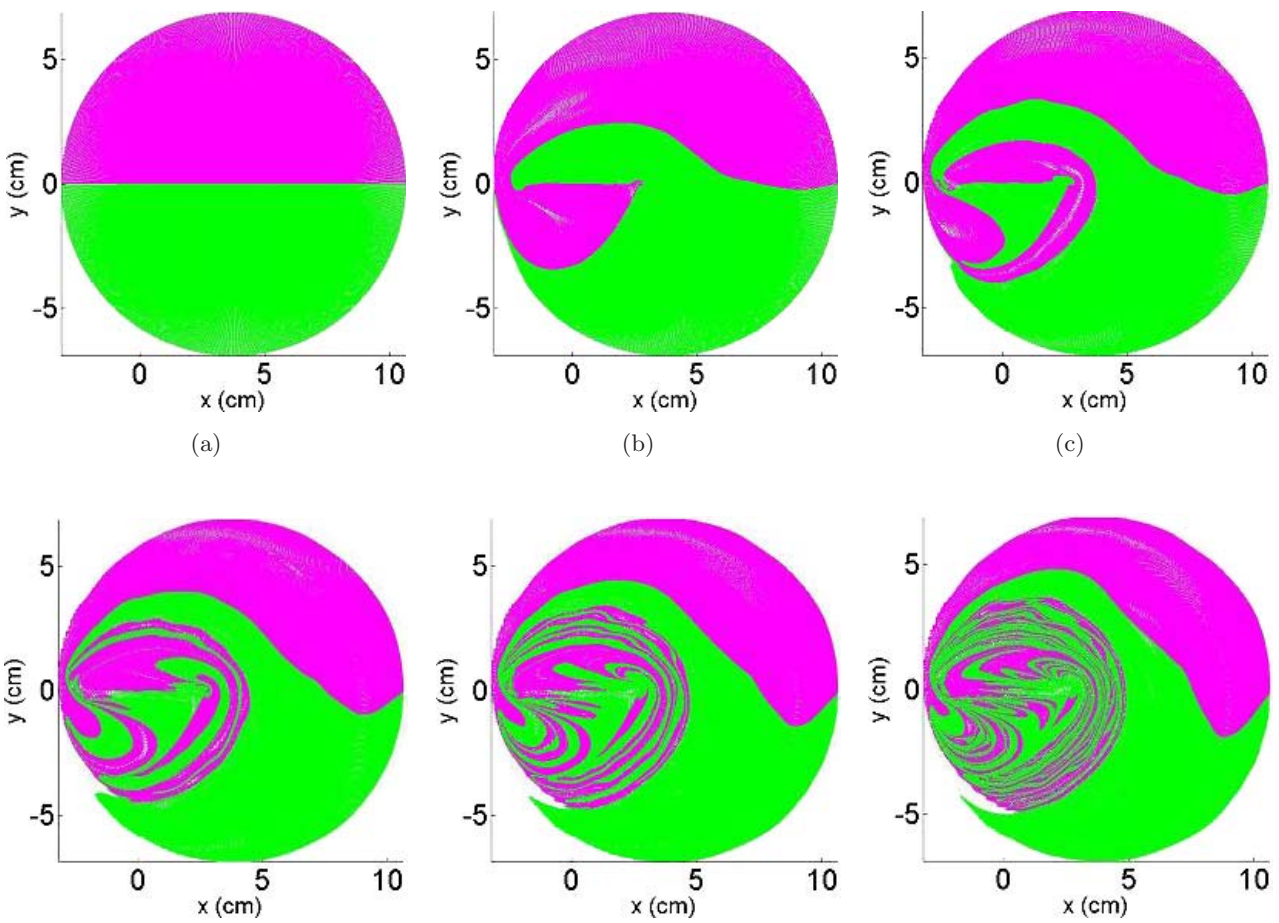


(a) (b) (c)

(d) (e) (f)

Fig. 9. Snapshots of particle tracers for the mixer with the centered blade. Two sets are particles, A (green) and B (magenta) are initially separated to occupy half of the physical space as shown (a). The initial particle distribution is then allowed to change as dictated by the flow field for 1, 2, 3, 4, and 5 periods, (b)–(f), respectively.

the centered-blade mixer. We verify these mixing behaviors again using the definition of mixing in Sec. 5.

## 4. Mathematical Model of the Mixers

This section is aimed to define a mathematical model of our mixing devices and we use it to investigate certain salient features of the FTLE fields of the mixing devices. We suppose that at time $t = 0$ the velocity field is constructed from a vorticity field under assumption of two-dimensional flow that the vorticity field is given by a vertical vorticity, $\omega = \omega_z$. Hence, we solve the Poisson's equation of the stream-function:

$$\begin{aligned} \Delta H &= -\omega_z \quad \text{on } \Omega, \\ u &= 0 \quad \text{on } \Omega. \end{aligned} \tag{6}$$

Here $\Omega$ is the circular boundary of the mixer (radius = 7.0) and $H$ is the Hamiltonian of the velocity field, that is,

$$\begin{aligned} \frac{dx}{dt} &= -\frac{\partial H(x,y)}{\partial y} \\ \frac{dy}{dt} &= \frac{\partial H(x,y)}{\partial x} \end{aligned} \tag{7}$$

We then recast the above time-independent system to a time-dependent system in a rotating frame using the change of coordinate

$$\begin{pmatrix} x \\ y \end{pmatrix} = \begin{bmatrix} \cos t & -\sin t \\ \sin t & \cos t \end{bmatrix} \begin{pmatrix} x' \\ y' \end{pmatrix}. \tag{8}$$

Now that we have developed a mathematical model for the mixer, we have to determine the vorticity $\omega_z$ that is well suited to replicate the important feature of the FTLE field of our mixing devices; that is the pseudo-barrier observed in the preceding section. We assume that the vorticity field $\omega_z$ is given by

$$\omega_z = G_0 - C(G_1 + G_2), \tag{9}$$

where

$$G_0 = \exp(-\sigma_0(\sigma_{0,x}x^2 + \sigma_{0,y}y^2))^{2m} \tag{10}$$

and

$$G_{1,2} = \exp(-\sigma_{1,2}(\sigma_{1x,2x}(x - s_{1,2})^2 + \sigma_{1y,2y}y^2))^2. \tag{11}$$

Here $C$ determines the relative magnitude of the vortices at the tips of the blade represented by the bivariate Gaussian function $G_1$ and $G_2$. The super-Gaussian function is used to replicate the vorticity due to the blade. Note the $G_0$ becomes a bivariate Gaussian function when $m = 1$. We vary the parameter $C$ to observe changes in the FTLE and fix the other parameters to $m = 2, \sigma_0 = 100, \sigma_{0,x} = 0.4, \sigma_{0,y} = 2.5, \sigma_1 = \sigma_2 = 400, s_1 = 0.5, s_2 = -0.5, \sigma_{1x} = \sigma_{2x} = 1.0$ and $\sigma_{1y} = \sigma_{2y} = 0.5$. Our specific choice of the form of Eqs. (10) and (11) and the values of the parameters is justified in Figs. 10 and 11, remembering that our goal here is to develop a model that contains the main topological features of the true system, which is simplifying but not necessarily predictive. Figures 10 and 11 show a comparison between the vorticity and velocity field of the given data and those numerically computed by Eq. (7).

Figure 12 illustrates the change in FTLE field at time $t = 0$ as $C$ is varied. First, we notice that the FTLE fields of our model have a similar LCS, or a transport pseudo-barrier, to that of the experimental data presented in the preceding section. Note that the FTLE fields of our numerical model also

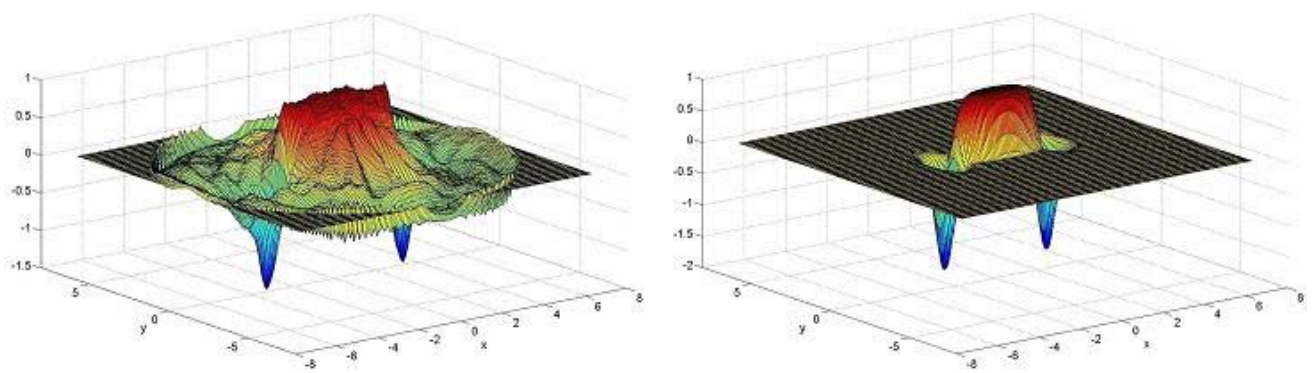

(a) (b)

Fig. 10. The vertical vorticity field, omegaz, of (a) experimental data and (b) analytic model using Eq. (9) with $C = 2.0$.

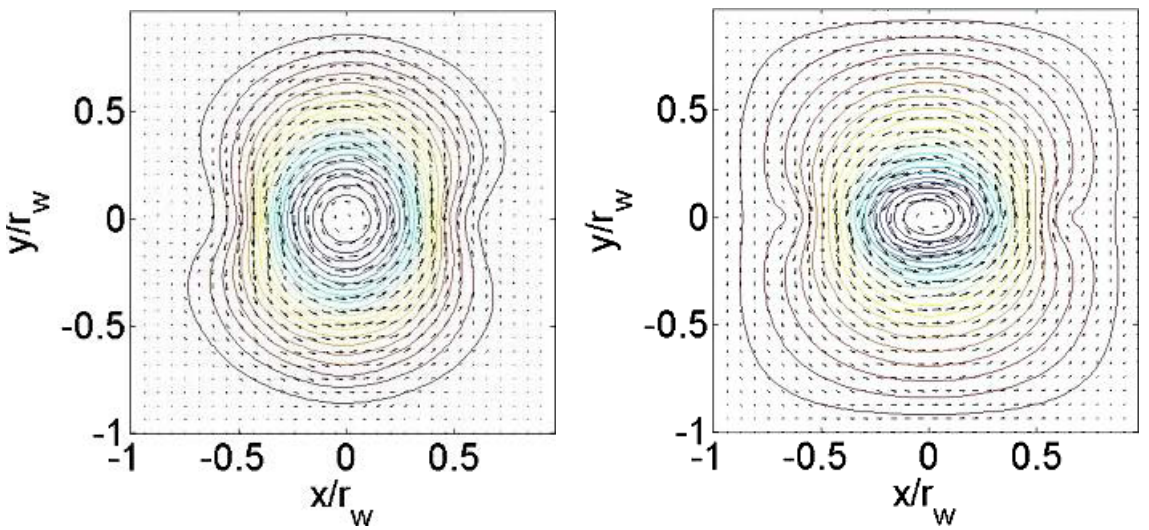


Fig. 11. The in-plane velocity field and representative streamlines for (a) experimental data and (b) analytical model with $C = 2.0$. Note the spatial dimensions have been normalized by the radius of the cylinder.

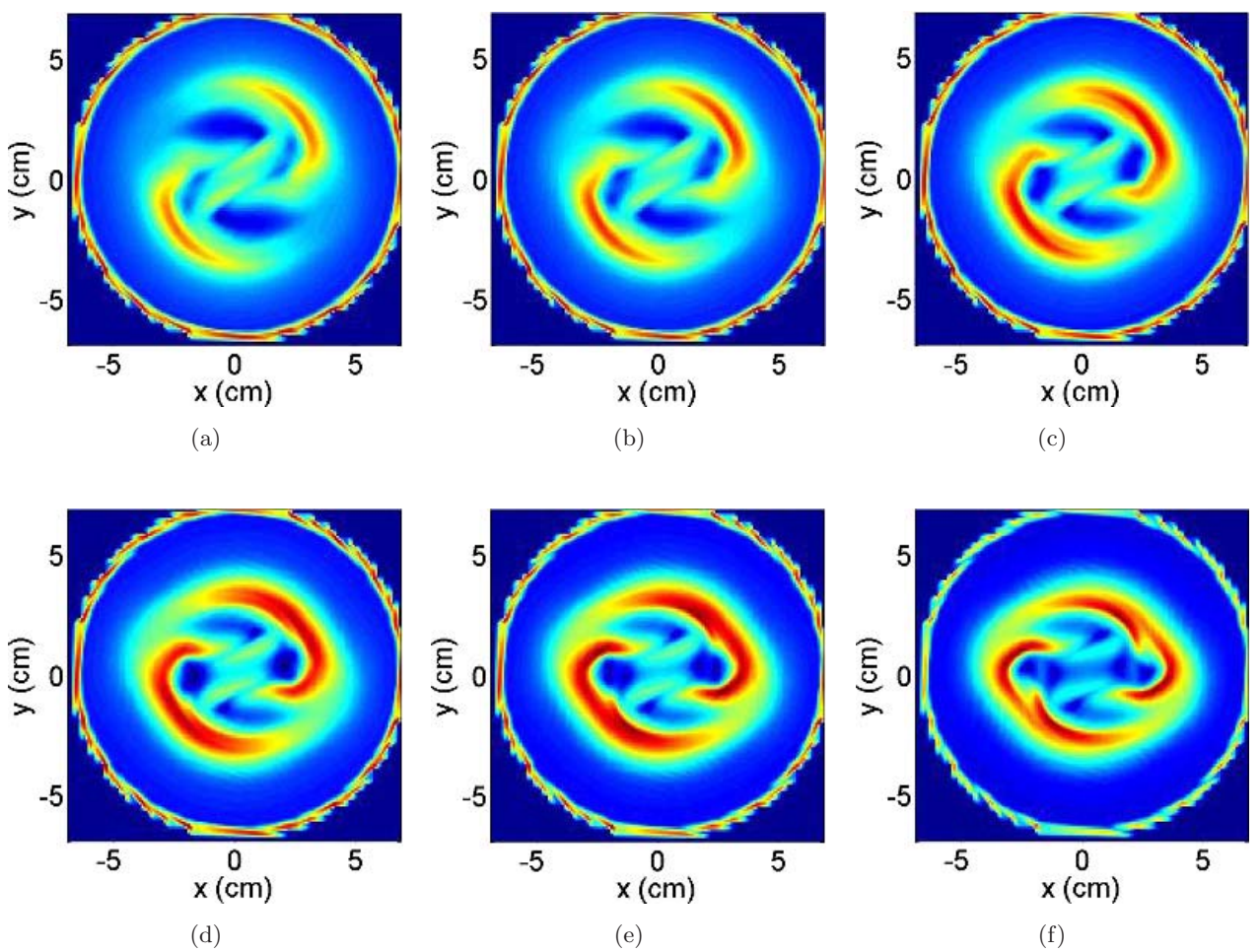


Fig. 12. The forward-time FTLE field at time $t = 0$ of the model Eq. (7) in a rotating frame. The parameter $C$ in the vorticity field Eq. (9) is varied to observe the change in the FTLE field. (a) $C = 0.5$, (b) $C = 1.0$, (c) $C = 1.5$, (d) $C = 2.0$, (e) $C = 2.5$, and (f) $C = 3.0$.

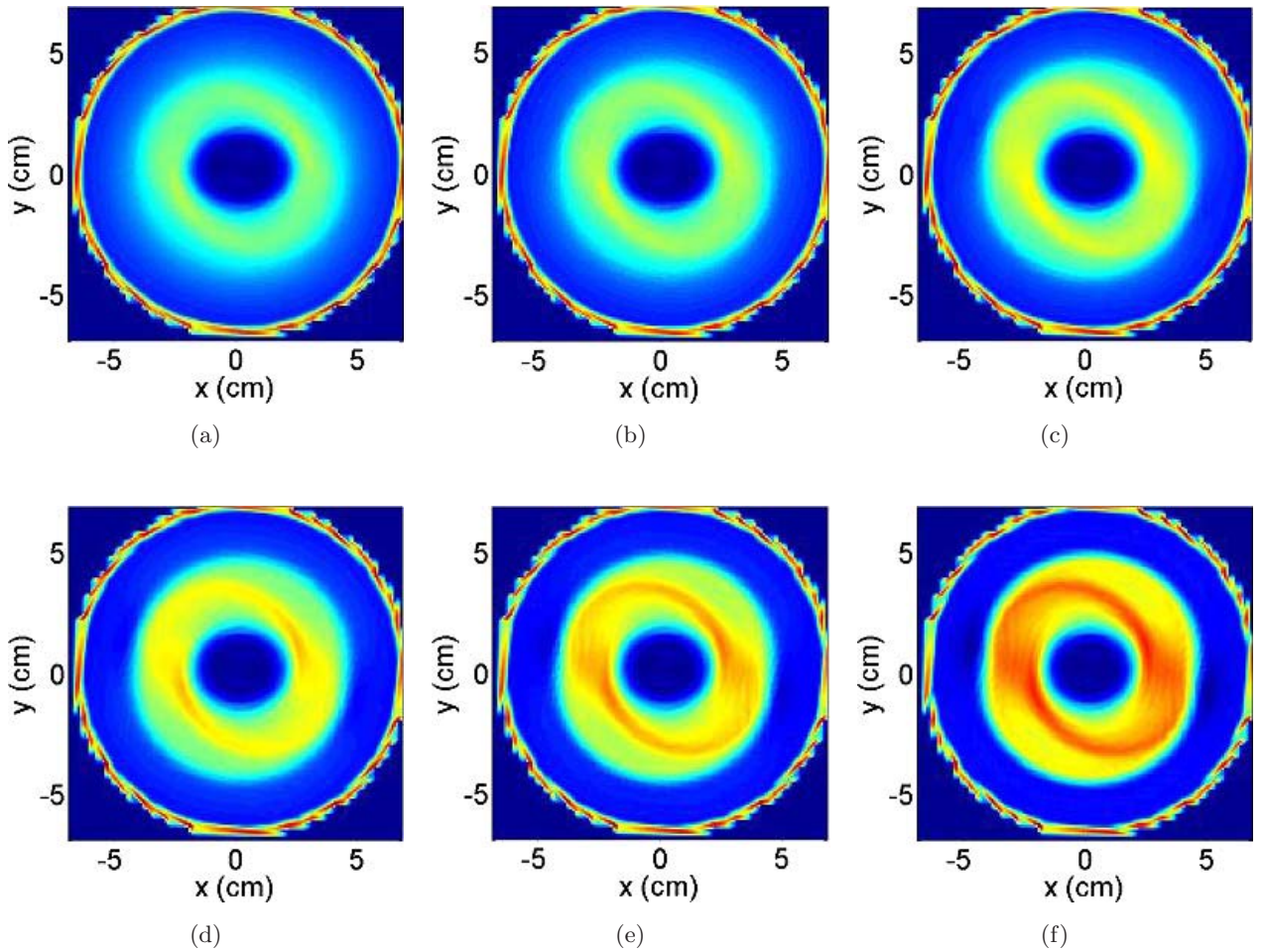


Fig. 13. The backward-time FTLE field at time $t = 0$ of the model Eq. (7) in a rotating frame. The parameter $C$ in the vorticity field Eq. (9) is varied to observe the change of the FTLE field. (a) $C = 0.5$, (b) $C = 1.0$, (c) $C = 1.5$, (d) $C = 2.0$, (e) $C = 2.5$, and (f) $C = 3.0$.

rotate in the same fashion as observed in the simulation of the real data and so we show here only the FTLE field at time $t = 0$. It is clear that the magnitude of the vortices near the tips of the blade are responsible for the strong barrier, which is in the region with large FTLE. Now, we observe the backward-time FTLE field of the model illustrated in Fig. 13. Again, as the magnitude of the vortices increases, the region with a large backward-time FTLE becomes more evident. Recall that the backward-time LCS signifies a generalization of an unstable manifold.

## 5. Mixing

For a study of mixing, consider first a measure of regions with mixing of the mixer with a centered blade. We initially divide the phase space into two distinct regions $A$ and $B$ as seen in Fig. 5(a). We will then proceed in a fashion closely motivated by the definition of a mixing system, which demands relative measures become asymptotically distributed [Sturman *et al.*, 2006]. We identify the particles initially located in $A$ species $S_a$, and similarly $S_b$ for those particles in $B$. We then partition the space $M$ into disjoint regions $R_i, i = 1, \ldots, N_R$, such that $M \subseteq \bigcup_{i=1}^{N_R} R_i$. Let $S = \{R_i : R_i \text{ contains both species } S_a \text{ and } S_b\}$. Finally, we define the ratio of the regions including both $S_a$ and $S_b$ by

$$R = \frac{\sum_{R_i \in S} \mu(R_i)}{\sum_i R_i}, \tag{12}$$

where the measure $\mu$ can be a Lebesgue (volume) measure. Clearly, the quality of mixing depends on the initial topology of sets $A$ and $B$. For the sets $A$ and $B$ initialized as in Fig. 5(a), the ratio $R$ at

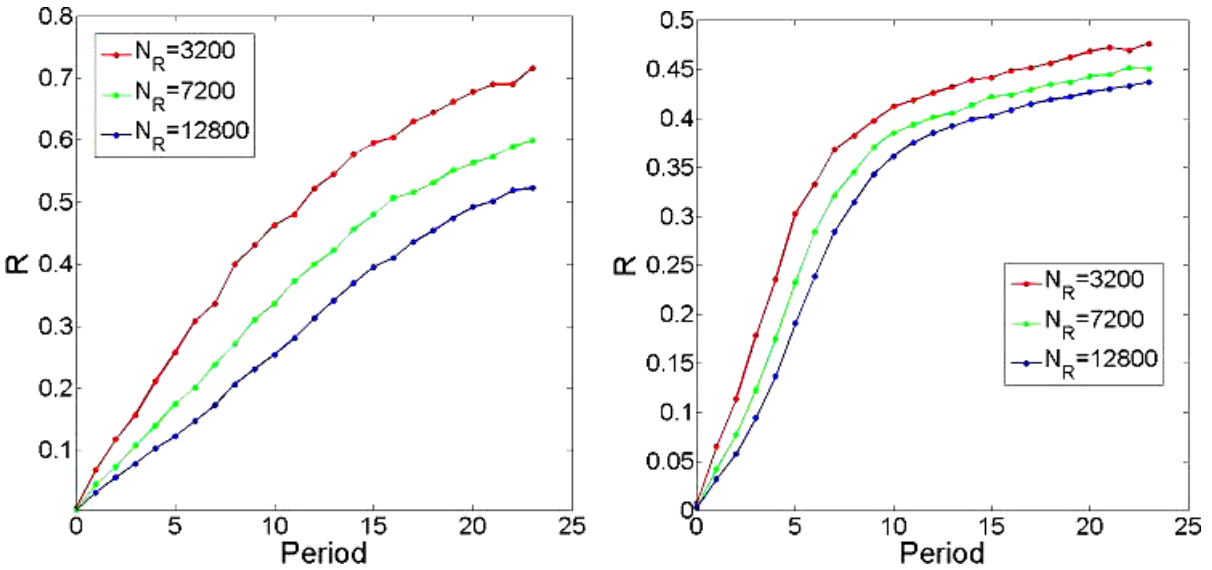


Fig. 14. The plot of the ratio $R$ in Eq. (12) at each period using different scales of $N_R$. (a) The mixer with a centered blade. (b) The mixer with an offset blade.

each period is given in Fig. 14 for different scales of $N_R$. These results agree with the behavior observed from the LCSs and tracers of the mixers in Sec. 3. Although the mixing rate of the offset-blade mixer is faster than that of the centered-blade, which can be observed by comparing the slope of the ratio $R$ between Figs. 14(a) and 14(b) at the early periods, the ratio $R$ becomes saturated since only the small region surrounded by the LCS, see Figs. 8 and 9, experiences a high degree of mixing.

## 6. Conclusion

We have demonstrated an application of the FTLE analysis for studying the transport behavior and the physics of mixing for our mixing devices. Particularly, we have extracted the time-varying Lagrangian structures of the mixing devices with different blade locations, which inhibit (passive) particle transport across the structures. Roughly speaking, the fluid particles initially separated by the LCS are not mixed with each other. Furthermore, we have shown by observing the numerical displacement of the tracers that the LCSs actually separate the region with a high degree of mixing from the region with the lower degree of mixing. By visualizing the LCSs and observing the transport behavior of the flow, we suggest a heuristic model of the trapping region formed by the transverse intersection of the stable and unstable manifolds of the periodic points, which physically corresponds to the blade tips. In addition, we have suggested a numerical model for our mixers and we have used it to study how the vorticity strength at the blade tips influences the LCSs. The results show that as the vorticity strength increases the LCSs become more evident, i.e. the heights of the FTLE ridges become larger. This results in more inhibited transport across these large pseudo-barriers. Finally, we have defined the notion of mixing that is appropriate to our work to investigate the mixing rate of two different mixing devices. We have shown that the results, based on this definition of mixing, agree with our observation of LCSs and particle tracers.

## Acknowledgments

The experiments used in this work were conducted at the Naval Surface Warfare Center Indian Head Division in Indian Head Maryland through the internal CORE research program. E. M. Bollt and N. Santitissadeekorn were supported under NSF-DMS-04 04778.

## References

Adrian, R. [2005] *Experim. Fluids* **39**, 159.
Bakalis, S. & Karwe, M. [2002] *J. Food Engin.* **51**, 273.
Bohl, D. [2007] *J. Fluids Engin.* **129**, 137.
Gendrich, C. & Koochesfahani, M. [1996] *Experim. Fluids* **22**, 67.
Haller, G. & Poje, A. C. [1998] *Physica D* **119**, 352.
Haller, G. [2000] *Chaos* **10**, 99.

Haller, G. [2002] *SPhys. Fluids A* **14**, 1851.
Jaffer, S., Bravo, V., Wood, P., Hrymak, A. & Wright, J. [2000] *Polym. Engin. Sci.* **40**, 892.
Shadden, S., Lekien, F. & Marsden, J. [2005] *Physica D* **212**, 271.
Shadden, S., Dabiriand, J. & Marsden, J. [2006] *Phys. Fluids* **18**, 271.
Sturman, R., Ottino, J. M. & Wiggins, S. [2006] "The mathematical foundations of mixing," *The Linked Twist Map as a Paradigm in Applications: Micro to Macro, Fluids to Solids* (Cambridge).
Tanguy, P., Bertrand, F., Labrie, R. & BritoDeLaFuente, E. [1996] *Chem. Engin. Res. Design* **74**, 499.
Wiggins, S. [2003] *Introduction to Applied Nonlinear Dynamical Systems and Chaos*, 2nd edn. (Springer).
Yoon, H., Hill, D., Balachandar, S., Adrian, R. & Ha, M. [2005] *Chem. Engin. Sci.* **60**, 3169.
Youcefi, A., AnneArchard, D., Boisson, H. & Sengelin, M. [1997] *J. Fluids Engin. — Trans. Asme* **119**, 616.
Zhou, G., Tanguy, P. & Dubois, C. [2000] *Chem. Engin. Res. Des.* **78**, 445.